Research on Chemical Intermediates
https://doi.org/10.1007/s11164-021-04538-z

Production, characterization, and application of a novel chitosan-g-maleic anhydride and modified graphene oxide nanocomposite, supported methane sulfonic acid, for efficient synthesis of 1-(benzothiazolylamino) methyl-2-naphtols

Nesa Lotfi Far[1] · **Esmael Rostami**[1] · **Ghasem Rezanejade Bardajee**[1]

Received: 7 May 2021 / Accepted: 5 July 2021

Abstract

An exceptionally productive and sustainable procedure is described in this paper to fabricate 1-(benzothiazolylamino) methyl-2-naphthols using a novel green nanocomposite of chitosan and diethylenetriamine-modified graphene oxide, supported methanesulfonic acid (Ch@GO-DETA.MSA.). For the synthesis of the nanocomposite, maleic anhydride was first attached to chitosan, and then, graphene oxide was modified by diethylenetriamine (GO@DETA). Subsequently, nanocomposite was prepared from the reaction of chitosan-g-maleic anhydride and GO@DETA. Finally, methane sulfonic acid was added to the nanocomposite to afford Ch@GO-DETA. MSA. Structural properties of the nanocomposite were explored through various techniques including X-ray diffraction (XRD), thermal gravimetric analysis (TGA), FTIR spectroscopy, scanning electron microscopy (SEM), and energy-dispersive X-ray spectroscopy (EDS). 1-(Benzothiazolylamino) methyl-2-naphthols were efficiently prepared in high to excellent yields through a multicomponent reaction of 2-aminobenzothiazole, aryl aldehydes, and 2-naphthol using Ch@GO-DETA.MSA. nanocomposite under solvent-free conditions. The proposed protocol exhibited superiority over several published protocols due to its nontoxicity and eco-friendly, catalytic ability, short reaction times, generality, efficiency, solvent-free condition, and simple workup.

Keywords Chitosan · Graphene oxide · 1-(Benzothiazolylamino) methyl-2-naphthols · Solvent-free synthesis · Nanocomposite · Nano-catalyst

✉ Esmael Rostami
Esmaelrostami@gmail.com; e.rostami@pnu.ac.ir

[1] Department of Chemistry, Payame Noor University, PO BOX, 19395-3697 Tehran, Iran

Published online: 26 July 2021

Introduction

Multicomponent reactions (MCRs) are among the valuable assets in medicinal chemistry, drug design, and drug exploration because of their high selectivity, efficiency, and simplicity [1]. The most important advantage of multicomponent reactions is that the target molecules do not need to be purified and the percentage of the by-products is very low. Multicomponent reactions can also decline the amount of required reactant, solvent, and cost [2–5].

Solvent-free reaction contributes to an ideal synthesis due to economic (high solvent price) and environmental (solvent risk to the environment) reasons. Moreover, rapid separation of products with no need for solvents will lead to faster reaction rates due to the thickening of the reactants in the absence of solvent. These points are of crucial significance during industrial production [6–8].

Chitosan is a polysaccharide composed of 2-amino-2-deoxy-D-glucopyranose and [1,4]-linked 2-acetamido-2-deoxy-D-glucopyranose. Chitin biopolymer is mainly extracted from marine sources with weak solubility in solvents. This problem can be resolved by partial deacetylation and the production of chitosan with higher solubility [9]. Nontoxicity, high adsorption capacity, good biodegradability, environmental compatibility, cost-effectiveness, multiple functional groups, efficient absorption of dyes and metals, rapid kinetics, and the ability to derive many derivatives are among the significant characteristics of chitosan. The properties of chitosan depend on its chemical nature including its degree of decontamination and deacetylation, molecular weight, crystallinity, and the ionic charge of amine functional groups [10, 11].

On the other hand, graphene oxide (GO) is a smooth sheet of carbon with extraordinary mechanical, electrical, and optical properties [12–14]. Furthermore, GO is nontoxic and possesses various functional groups, making it a valuable candidate for the removal of molecules and ions from aquatic environments. Graphene oxide can be dispersed in the chitosan matrix through the formation of amide linkages [15]. Chitosan is a natural polymer with distinctive characteristics including nonantigenicity, biological renewability, biodegradability, and biocompatibility [16–18]. Therefore, the functionalization of GO-DETA with chitosan-g-maleic anhydride is a promising approach for reaching a novel nanocomposite with exceptional properties of both materials.

Benzothiazole is an important heterocyclic system with critical significance in organic synthesis and medicinal chemistry. These heterocyclic compounds form the structural unit of numerous drugs such as astemizole [19], albendazole [20], omeprazole [21], and mebendazole [22]. Benzothiazole derivatives have shown considerable features including antimalarial [23], antifungal [24], anti-tubercular [25], anti-infective and herbicide [26], anticancer [27], and antimicrobial [28] activities. For this purpose, diverse catalysts containing [Fe_3O_4@SiO_2@$(CH_2)_3$-urea-SO_3H/HCl] [29], RHA-[pmim]HSO_4 [30], agar [31], ultrasound-promoted, H_2O/HPA [32], [PVP-SO_3H] HSO_4 [33], and $NaHSO_4.H_2O$ [34] have been utilized for the production of 1-(benzothiazolylamino) methyl-2-naphthols. These procedures suffer from a series of disadvantages such as elevated temperatures

and severe processes, toxic and expensive catalysts, long duration, need for poisonous solvents, huge amounts of by-products, and tedious workup. Thus, research on exploring novel protocols for the synthesis of mentioned heterocycles has gained significant attention.

In this study, the productive construction of 1-(benzothiazolylamino) methyl-2-naphthols as biologically active products was studied using a green and sustainable nanocomposite produced from chitosan and graphene oxide derivatives. The protocol follows green chemistry principles including solvent-free conditions, efficient reaction rates, higher yields, nontoxicity, inexpensive promoter, and moderate conditions.

Results and discussion

In this research, partially N-maleated chitosan [35] and diethylenetriamine-functionalized graphene oxide nanocomposite [36] were prepared and activated using methane sulfonic acid. The resulting nanocomposite was successfully used as an environmentally benign catalyst in a multicomponent one-pot process for the synthesis of 1-(benzothiazolylamino) methyl-2-naphthols under solvent-free conditions. To examine the stability and durability of the nanocomposite, it was successively recovered and reused for five runs. The process exhibited a series of advantages including the use of carbon and biopolymer-based nanocomposite (catalyst), solvent-free condition, absence of toxic metals, and easy storage and handling of catalyst.

Production of graphene oxide and diethylenetriamine-functionalized graphene oxide

Graphene oxide was produced according to the improved Hummers method (Scheme 1) [37, 38]. To obtain exfoliated graphene oxide with single-layer structure through purification process, after elimination of solvent using a centrifuge, deionized water was utilized and the mixture was sonicated for 30 min. The obtained colloid was purified with a centrifuge to offer nanostructured graphene oxide. Diethylenetriamine-functionalized graphene oxide (GO@DETA) was prepared from graphene oxide and diethylenetriamine using dicyclohexylcarbodiimide (DCC) and trimethylamine as reagents (Scheme 1) as previously reported [36].

Preparation of partially N-maleated chitosan and diethylenetriamine-functionalized graphene oxide (Ch@GO-DETA) nanocomposite

N-Maleated chitosan was synthesized as reported in [35] using chitosan and maleic anhydride (Scheme 2). The nanocomposite was prepared from the reaction of maleated chitosan and GO@DETA using EDC (Scheme 2). The reaction was performed for 24 h in NMP at 130 °C. The final nanocomposite was purified via

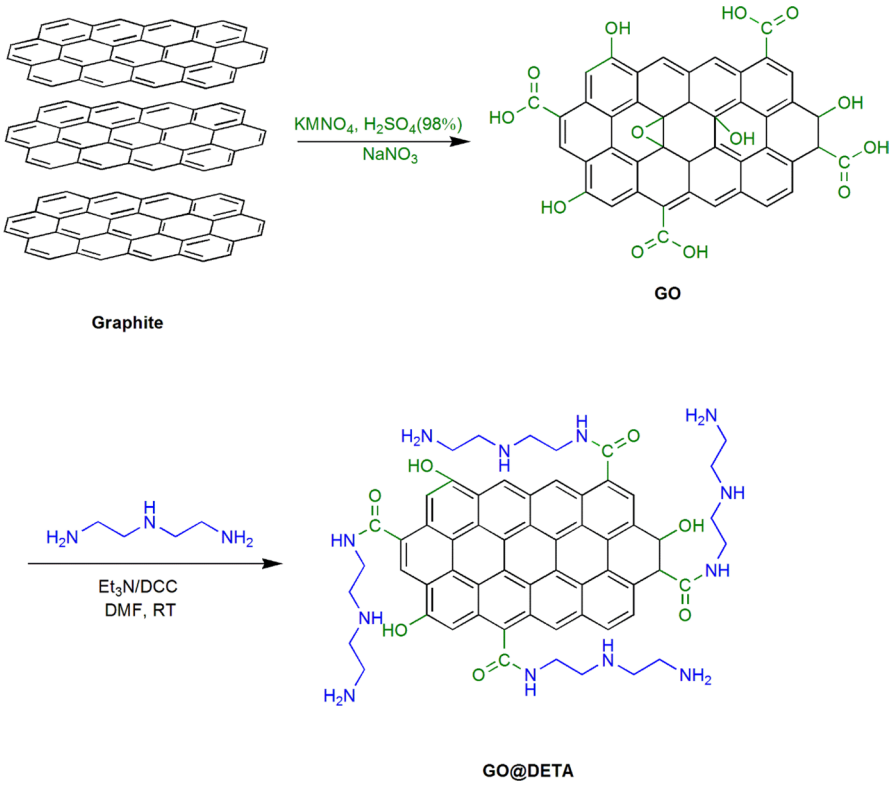

Scheme 1 The synthesis of GO@DETA

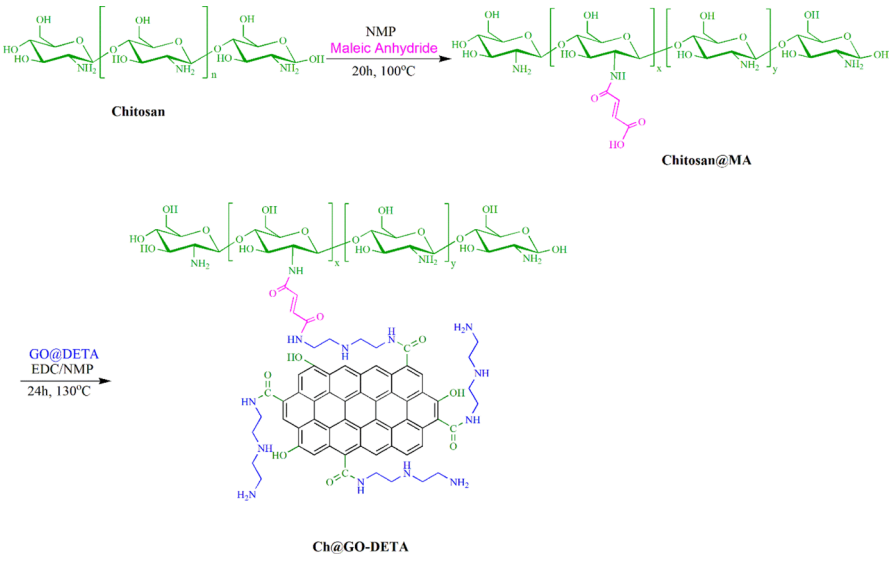

Scheme 2 The synthesis of Ch@GO-DETA

centrifugation and washing with deionized water and hot ethanol. Finally, purified and dried nanocomposite was reached at low pressure at 50 °C.

Preparation of chitosan, diethylenetriamine-functionalized graphene oxide, and methane sulfonic acid nanocomposite (Ch@GO-DETA.MSA)

The above-mentioned nanocomposite (Ch@GO-DETA) was dispersed in chloroform and ultrasonically treated to reach a colloidal solution. Then, methane sulfonic acid was used and the reaction continued for 5 h. Ultimately, the purified product (Ch@GO-DETA.MSA) was provided via centrifugation and washing with chloroform solution to remove unreacted and physically adsorbed acids (Scheme 3). Ultimately, the nanocomposite was dried at 50 °C at low pressure.

Characterization of nanocomposites

Characterization of Ch@GO-DETA and Ch@GO-DETA.MSA nanocomposites was appropriately performed by various techniques including FTIR, EDX, FESEM, XRD, TG, and DSC.

FTIR spectra

FTIR spectra of graphene oxide, GO@DETA, Ch@GO-DETA nanocomposite, and Ch@GO-DETA.MSA nanocomposite are presented in Figs. 1 and 2. Accordingly, the FTIR spectrum of GO shows bands related to various structural substituents (Fig. 1a). The bands at 1068 and 1178 cm^{-1} demonstrate ether groups. Also, the bands at 1286 and 1577 cm^{-1} are indicative of the double bonds of aromatic rings. Stretching vibrations of carbonyl groups of graphene appeared at 1720 cm^{-1}

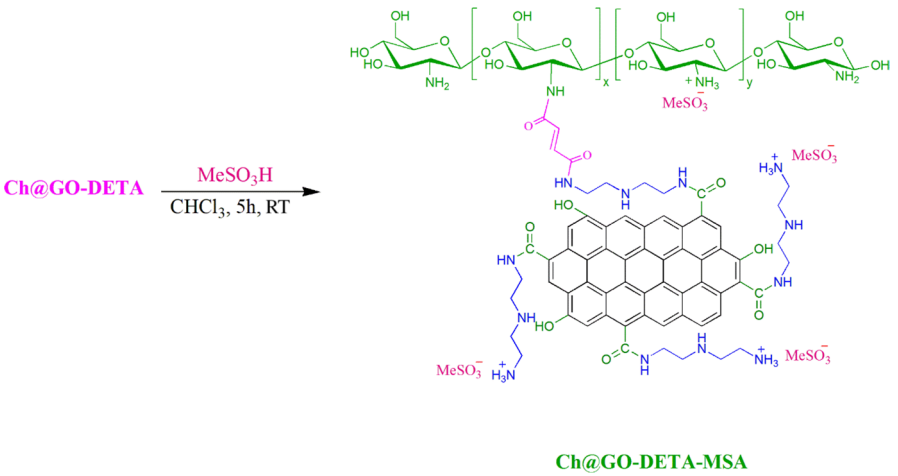

Scheme 3 The synthesis of Ch@GO-DETA.MSA

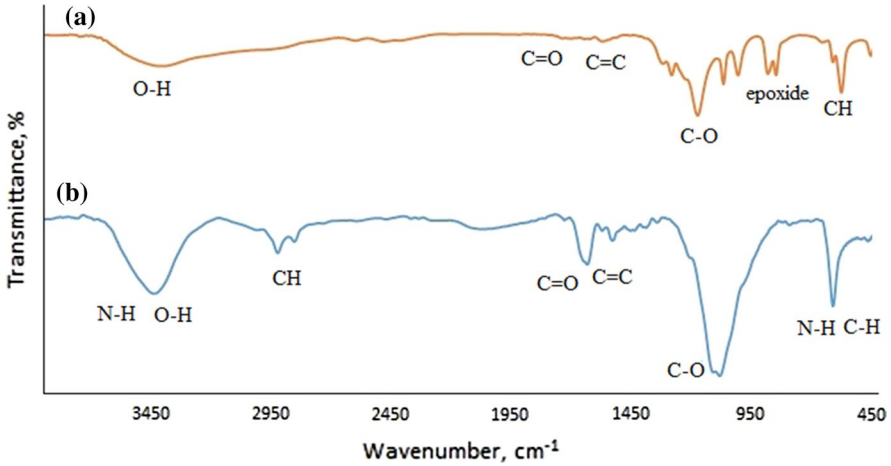

Fig. 1 The FTIR spectra of (**a**) GO and (**b**) GO@DETA

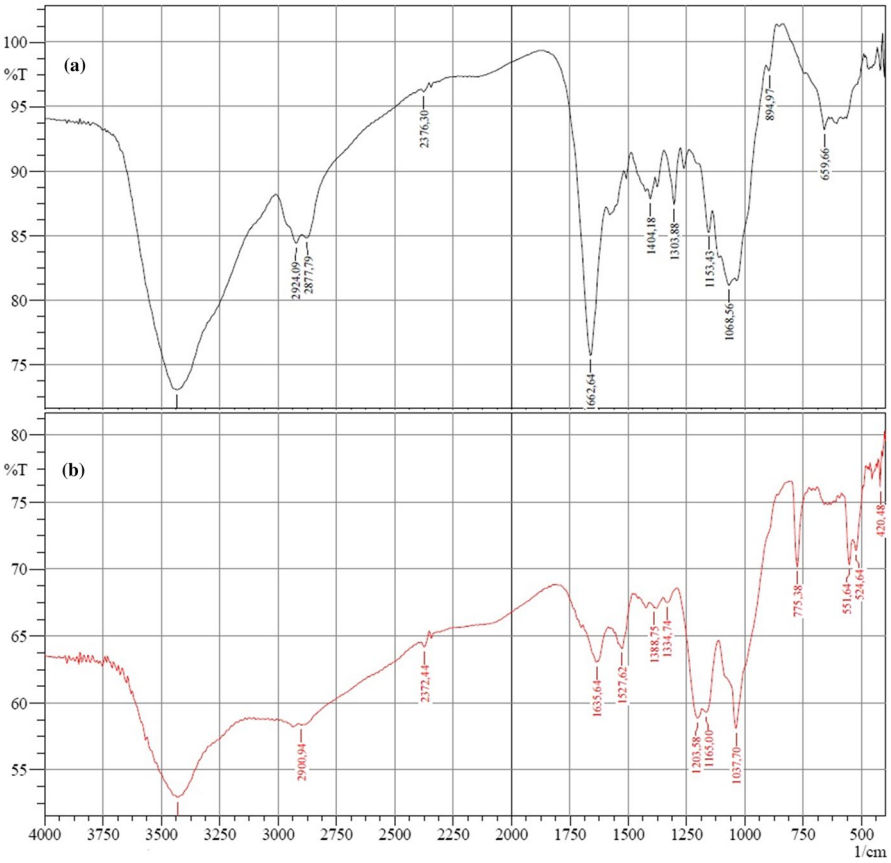

Fig. 2 The FTIR spectra of **a** Ch@GO-DETA and **b** Ch@GO-DETA.MSA nanocomposites

[39]. Furthermore, OH of alcoholic, phenolic, and acidic functional groups can be observed at 3418 cm^{-1} as stretching vibrations. The epoxide vibrations probably emerged at 844 and 876 cm^{-1}. Moreover, CH bending vibrations can be related to 567 cm^{-1} band [40].

Figure 1b depicts the FTIR spectrum of GO@DETA. The stretching vibrations of NH and OH functional groups in graphene oxide and diethylenetriamine moieties appeared as a strong band around 3437 cm^{-1}. Aliphatic CH vibrations of diethylenetriamine can be observed at 2857 and 2926 cm^{-1} [41]. Further, stretching vibrations of double bonds of graphene structure appeared at 1635 cm^{-1}. Also, stretching vibration of the carbonyl groups of graphene oxide appeared at 1696 cm^{-1}. Furthermore, strong stretching vibrations of etheric groups can be identified at 1082 and 1097 cm^{-1} [16]. Additionally, a band at 612 cm^{-1} can be assigned to diethylenetriamine NH or bending vibrations of aromatic double bonds on the GO@DETA surface. This vibration is stronger compared to GO. Functionalization of graphene oxide can be confirmed by aliphatic CH vibrations of diethylenetriamine in GO@DETA at 2857 and 2926 cm^{-1}. Furthermore, upon functionalization, graphene oxide skeleton converted to graphene benzene rings with smooth structure as indicated by stronger C=C vibrations in FTIR spectrum of GO@DETA. Another evidence for functionalization of graphene is the redshift (bathochromic shift) of carbonyl band at GO@DETA compared to GO, which shows the formation of amide functional groups (Fig. 1a and b).

According to the FTIR spectrum of Ch@GO-DETA in Fig. 2a, broad and strong stretching vibrations around 3430 cm^{-1} correspond to NH and OH vibrations in the amide groups of chitosan and graphene oxide and diethylenetriamine and intramolecular hydrogen bonds [42]. Also, aliphatic CH symmetric and asymmetric stretching vibrations in chitosan and diethylenetriamine appeared at 2924 and 2877 cm^{-1} [42]. These bands are the fingerprints of polysaccharides that appeared in FTIR spectra of carrageenans, glucans, and xylan [43]. The presence of amides carbonyl groups in GO@DETA and maleimide was established by vibration stretching bands at around 1662 cm^{-1} and higher frequencies [43]. Further, bands at 1560 correspond to NH of amide group [44]. Moreover, bands at 1404 and 1308 cm^{-1} can be attributed to aromatic double bonds. The band around 1423 cm^{-1} indicates CH_2 moiety. C–O–C etheric vibration bands in chitosan structure emerged at 1153 cm^{-1} [43]. Additionally, the bands at 1029 and 1068 cm^{-1} can be assigned to stretching vibrations of etheric groups in chitosan and graphene oxide [43]. Furthermore, the band at 659 cm^{-1} can be related to the bending vibrations of NH or aromatic double bonds. The out-of-plane bending vibration of CH in the polysaccharide ring appeared at 894 cm^{-1} [43].

FTIR spectrum of Ch@GO-DETA.MSA is shown in Fig. 2b. The band related to the stretching vibrations of OH, NH, and hydroxyl of the SO_3H group can be seen at 3400 cm^{-1} [45]. Stretching vibrations of CH in polysaccharide rings and diethylenetriamine moieties can be observed at 2876 and 2924 cm^{-1} [45]. The absorption bands at 1695 cm^{-1} can be assigned to vibrations of carbonyl bonds of amides on the graphene oxide surface [46]. A strong band at 1635 cm^{-1} corresponds to maleimide and chitosan (acetyl) carbonyl bonds and NH_3^+ groups on chitosan and graphene oxide [47]. Stretching vibrations of C=C in graphene can be observed at

1527 cm^{-1}. The absorption band at 1334 cm^{-1} can be regarded as a sign of C–N amide bond vibration. The small bending vibration of N–H bonds can be seen at 1550 cm^{-1} [44]. The CH_2 vibrations can be seen at ~ 1420 cm^{-1} [45]. The CH_3 symmetrical vibrations emerged at ~ 1388 cm^{-1}. The band observed at 1203 cm^{-1} can be assigned to vibrations of C–O etheric groups in graphene oxide and chitosan [48]. Asymmetric stretching vibrations of C–O–C chitosan ring [43] and SO_3 group [45] can be observed at 1165 cm^{-1}. Also, the bands of etheric [45] or SO_3 [49] can be seen at 1037 and 1065 cm^{-1}. Moreover, the out-of-plane bending vibrations of CH in the chitosan ring can be seen at 890 cm^{-1} [43]. Furthermore, NH or C–S bending vibrations can be detected at 775 cm^{-1} [49]. As well, bands of SO_3 group can be determined at 524 and 551 cm^{-1} [49].

XRD spectra

XRD patterns of GO, GO@DETA, Ch@GO-DETA, and Ch@GO-DETA.MSA are reported in Figs. 3 and 4. Graphene oxide showed two characteristic peaks at $2\theta = 9.55°$ and 20.5°. The former corresponds to graphene oxide, while the latter indicates trace amounts of reduced graphene oxide (Fig. 3a). Reduced graphene oxide was probably formed through exfoliation process in an ultrasonic bath for preparation of single-layer nanostructured graphene oxide. Figure 3b reports the XRD pattern of GO@DETA. As seen, the peak at 9.55° disappeared and new peaks emerged at 15°–32° corresponding to new crystalline structures with various d-spacings. This phenomenon shows the effect of functionalization on the crystallinity of graphene oxide. Functionalized graphene oxide exhibited higher crystallinity compared with pristine graphene oxide.

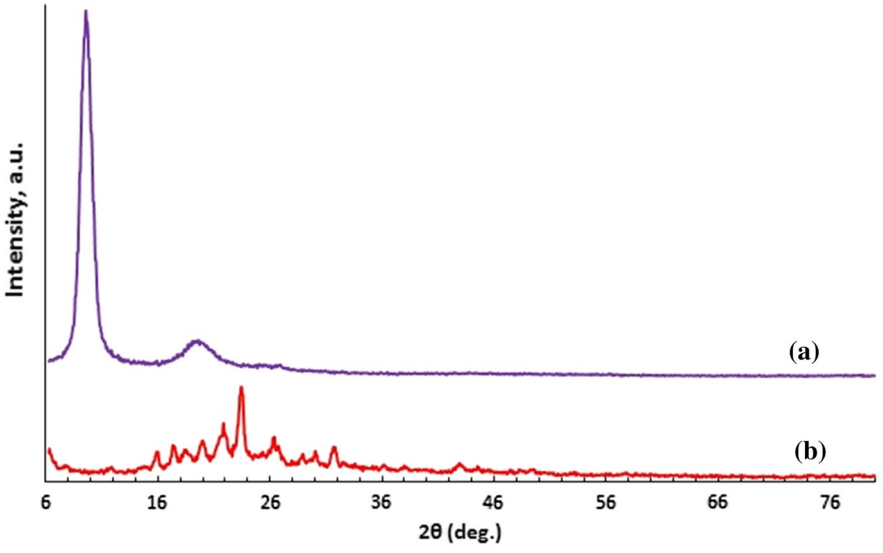

Fig. 3 XRD spectra of GO (**a**) and GO@DETA (**b**)

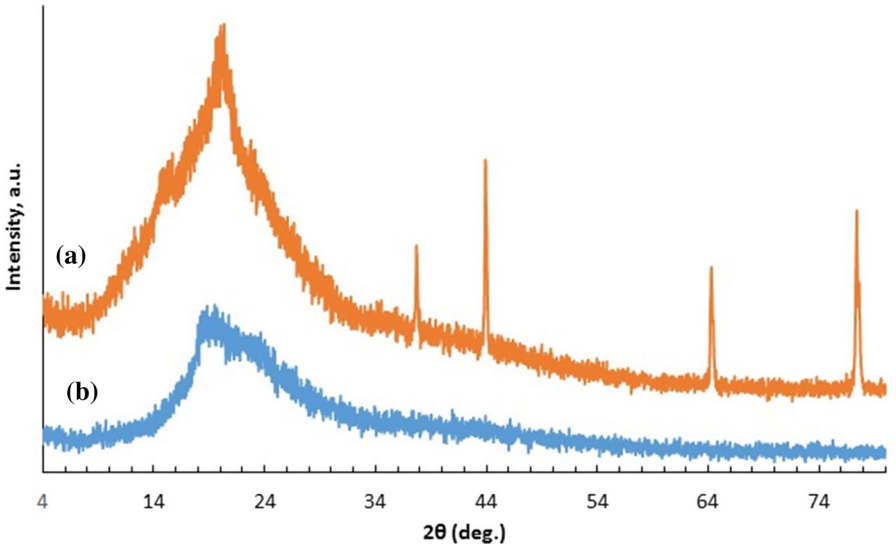

Fig. 4 XRD patterns of Ch@GO-DETA (**a**) and Ch@GO-DETA.MSA (**b**)

XRD pattern of Ch@GO-DETA nanocomposite (Fig. 4a) shows a broad peak in the range of 10°–50°, indicating the amorphous structure of nanocomposite. According to the XRD pattern of chitosan and reduced graphene oxide with broad peaks in this area [50, 51], the structure of Ch@GO-DETA nanocomposite is mainly amorphous. Several sharp peaks at 39°, 43°, 64° and 78° showed the partial crystalline structure of Ch@GO-DETA nanocomposite. Thus, the XRD pattern confirmed the presence of chitosan and reduced graphene oxide in the nanocomposite structure [52].

The XRD pattern of the Ch@GO-DETA.MSA nanocomposite is observed in Fig. 4b. The amorphous structure can be confirmed due to the wide peaks in Ch@GO-DETA.MSA nanocomposite as verified by chemical sources [53].

FESEM images and EDS analysis

The Ch@GO-DETA and Ch@GO-DETA.CH_3SO_3H samples were examined using FESEM analysis (Fig. 5). According to the images, the particle sizes lie between 17–33 and 17–42 nm for Ch@GO-DETA (Fig. 5a) and Ch@GO-DETA.MSA (Fig. 5b) nanocomposites, respectively. Also in both combinations, some levels of uniformity were observed.

EDS analysis was utilized to explore elemental composition. The results are demonstrated in Fig. 6, which confirmed the presence of C, N, and O on the GO@DETA. As expected, the EDS spectrum of Ch@GO-DETA showed C, N, and O elements (Fig. 7a), while C, N, O, and S were detected in Ch@GO-DETA.MSA nanocomposite (Fig. 7b).

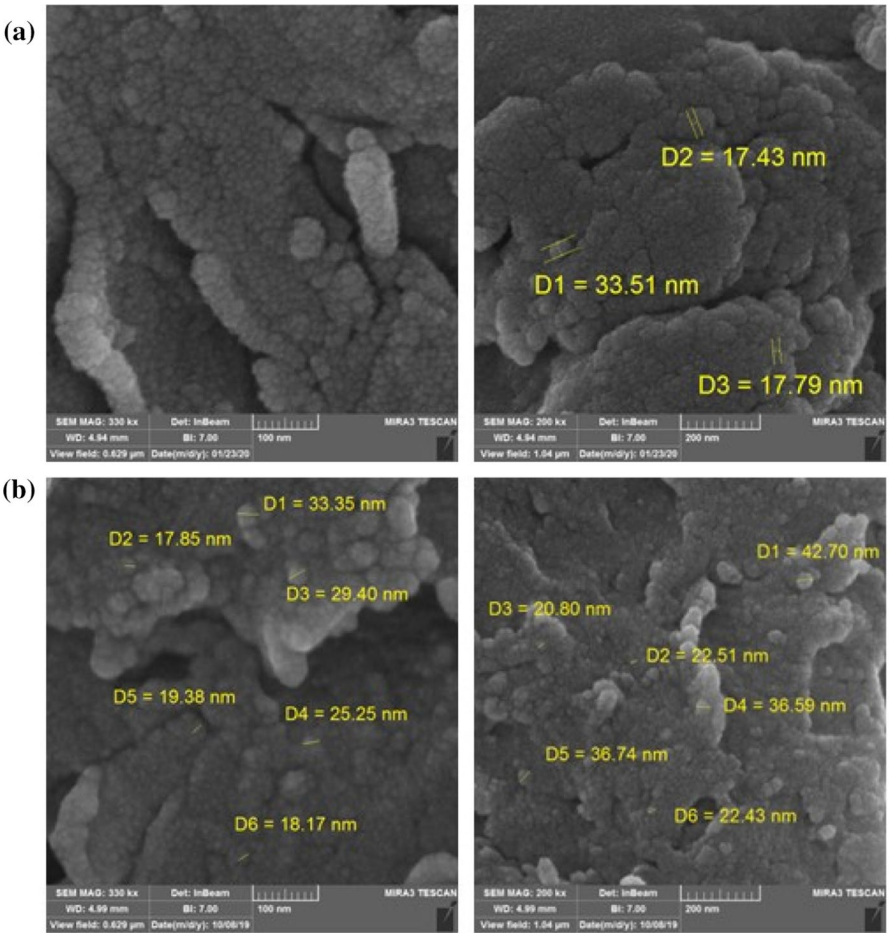

Fig. 5 SEM images of (**a**) Ch@GO-DETA, (**b**) Ch@GO-DETA.MSA

TGA, DTG, and DTA analysis of nanocomposite

Thermogravimetric analysis (TGA) and differential thermogravimetric analysis (DTG), as well as differential thermal analysis (DTA), were employed to study the thermal behavior of Ch@GO-DETA.MSA nanocomposite. The sample was heated to 600 °C. The TGA diagram is shown in Fig. 8. According to the TGA results, the catalyst is thermally stable up to 200 °C, making it suitable for applications at temperatures as high as 200 °C. According to the DTG diagram (a derivative of the TGA diagram), there are four regions of structural decomposition and weight loss; the largest one was seen at 214 °C [52]. Presumably, water and solvents evaporate in the first weight loss at 74–100 °C. The weight loss at 214 °C can be related to the loss of functional groups of chitosan [54]. The

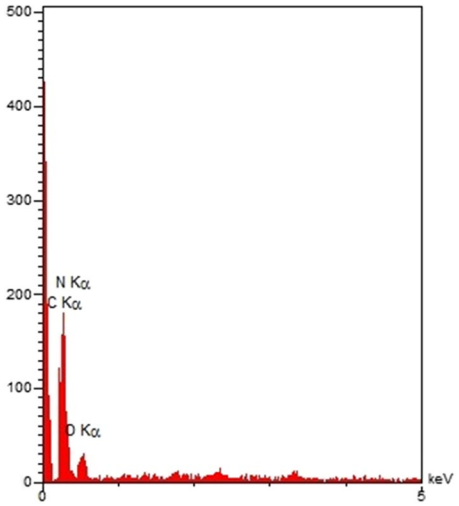

Fig. 6 EDX analysis of GO@DETA

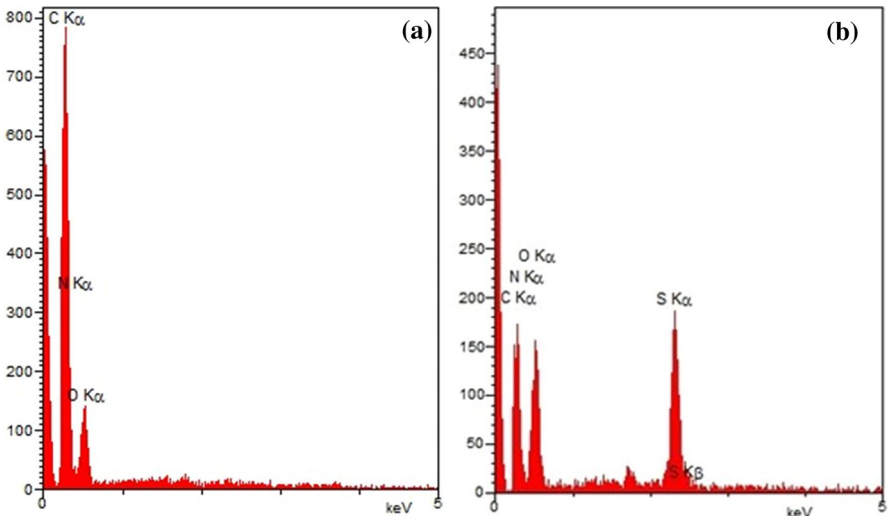

Fig. 7 EDX analysis of (**a**) Ch@GO-DETA, (**b**) Ch@GO-DETA.MSA

weight variations at 319 and 461 °C can be also assigned to the degradation of the polymer and graphene structure. The amount of weight loss was 65.43% and the residual yield was 34.57%, which indicates the stability of the sample. The DTA diagram showed two endothermic reactions at 207 and 321 °C. Comparing the TGA diagram with the DTA results, these two reactions are the isolation of functional groups from the surface and destruction of chitosan and graphene structures, respectively (Fig. 8).

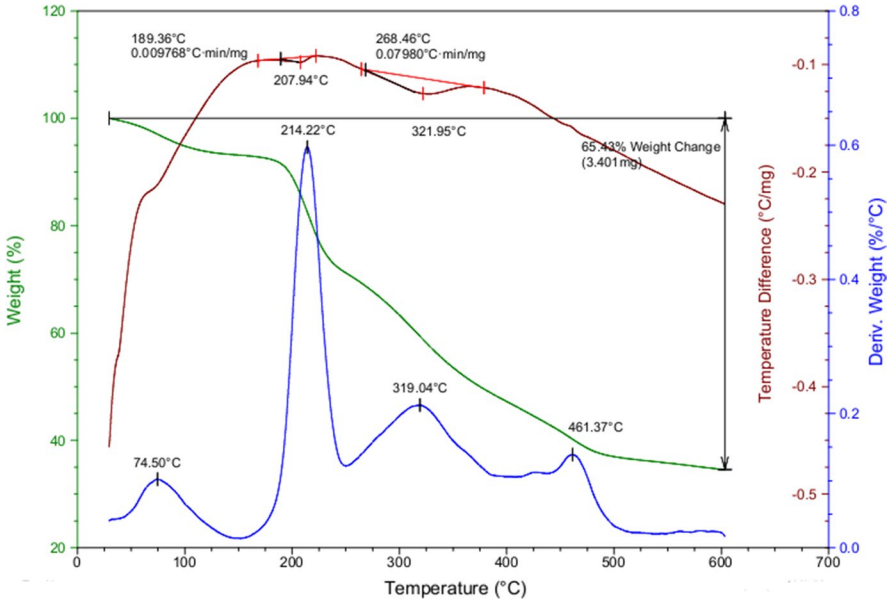

Fig. 8 TGA, DTG, and DTA diagrams of Ch@GO-DETA.MSA

Synthesis of 4-[4-(4-chlorophenyl)-3-aza-2-oxo-propyloxy] benzaldehyde (3)

To prepare a new 1-(benzothiazole amino) methyl-2-naphthol (**7n**), first, a new aldehyde derivative (**3**) was prepared from N-(4-bromophenyl)-2-chloroacetamide (**1**) [55] and 4-hydroxy benzaldehyde (**2**). The reaction proceeded in acetonitrile under reflux conditions (Scheme 4). FTIR, ^{1}H NMR, ^{13}C NMR, and mass spectroscopy were employed to define the structure of **3**. Based on the FTIR spectrum, the NH band of the amine group can be seen at 3541 cm^{-1}, while the stretching vibration of phenolic hydroxide emerged at 3398 cm^{-1}. Moreover, C=O vibration can be detected at 1689 cm^{-1} and the aromatic double-bond vibrations are manifested at 1593, 1534, and 1442 cm^{-1}. Furthermore, the bands at 1176 and 742 cm^{-1} can be assigned to the vibration of etheric (C–O) and aromatic C–Cl groups, respectively. ^{1}H NMR spectrum showed two protons for methylene, eight protons for the aromatic region, one proton for aldehyde, and one proton for amide NH. On the other hand, ^{13}C NMR exhibited one aliphatic carbon, 12 aromatic carbons, and two carbonyl carbons for the amide carbonyl group and the aldehyde group. Thus, NMR spectra

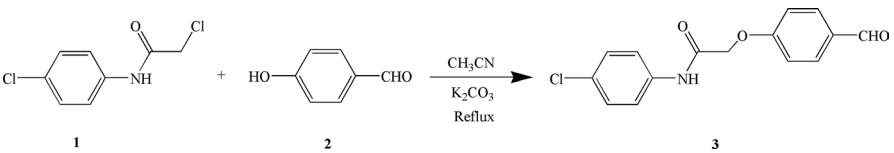

Scheme 4 Synthesis of **3**

confirmed the structure of **3**. Furthermore, the mass spectrum verified the molecular weight of **3** at m/z of 290 equivalent to $(M+1)^+$.

Optimum conditions for the production of 1-(benzothiazolylamino) methyl-2-naphtols and scope of nanocomposite (catalyst)

For optimization, the reaction of 2-aminobenzothiazole, 4-chloro benzaldehyde, and 2-naphthol using nanocomposite (Ch@GO-DETA.MSA) was selected as a model (Scheme 5). The process was carried out under diverse conditions, and the impacts of five variables (time, the reaction temperature, catalyst load, type of catalyst, and solvent (or solvent-free condition)) were investigated. Ultimately, the optimum reaction conditions involved the temperature of 80 °C using 0.028 g nanocomposite under solvent-free medium for 10 min (Table 1, entry 5).

Thin-layer chromatography (TLC) (n-hexane/ethyl acetate, 4:1) was selected to monitor the improvements. After cooling, the residue was dispersed in hot alcohol and the nanocomposite was separated and the precipitate was washed with ethyl acetate (3 × 15 mL) to yield the product. To study the generality of our nanocomposite, diverse aldehydes were selected and the process was carried out under optimal conditions to reach desired product (Scheme 6). Aromatic aldehydes with various substituents including benzaldehyde (with no substituent), electron-releasing and electron-accepting groups, or halogens were run with 2-aminobenzothiazole and 2-naphtoles and investigated in the presence of Ch@GO-DETA.MSA nanocomposite (Table 2). According to the findings, aldehydes with electron-withdrawing groups and halogens afforded higher yields of products as compared to the electron-donating groups.

To confirm the structure of products, the melting points of previously reported ones were measured and weighed up to the data reported elsewhere. On the other hand, NMR spectroscopic methods and FTIR and elemental analysis were utilized for some of them to identify their structures. ^{1}H NMR spectrum of **7b** showed 14 protons for the aromatic region and one methine proton, as well as one NH proton for benzothiazole and one hydroxyl proton of 2-naphthol. Also, ^{13}C NMR spectrum determined one methine carbon and 22 carbons for aromatic region. Thus, NMR

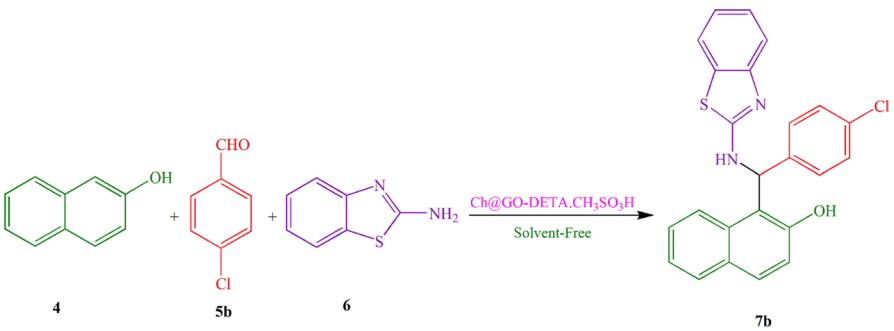

Scheme 5 The model reaction for the synthesis of **7b**

Table 1 Optimization of the nanocomposite loading, temperature, and time for the synthesis of 7b

Entry	Ch@GO-DETA. MSA (g)	Solvent	Temp. (°C)	Time (min)	Yield[a] (%)
1	–	–	90	90	40
2	0.040	–	90	10	87
3	0.028	–	90	10	95
4	0.020	–	90	30	90
5	0.028	–	80	10	95
6	0.028	–	70	30	95
7	0.028[b]	–	80	10	44
8	0.028[c]	–	80	10	48
9	0.028[d]	–	80	10	53
10	0.028	EtOH	70	80	55
11	0.028	H_2O	80	80	72
12	0.028	$CHCl_3$	50	60	56
13	0.028	CH_3CN	70	80	60

[a]Isolated yield

[b]GO

[c]GO@DETA

[d]Ch@GO-DETA

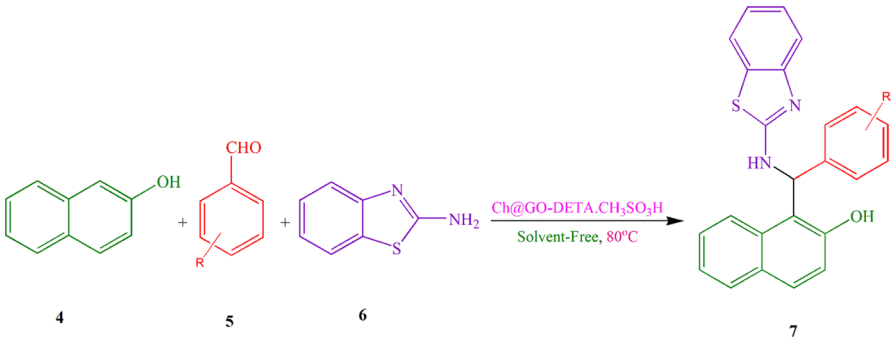

Scheme 6 Production of 1-(benzothiazolylamino) methyl-2-naphtols

spectroscopy confirms the structure of **7b**. Moreover, ^{1}H NMR spectrum of **7l** reported 15 protons for aromatic region and methine group as multiplet in addition to one proton for benzothiazole NH and one proton for 2-naphthol hydroxyl group.

Furthermore, the FTIR spectrum of **7m** showed stretching vibration of NH and OH at 3368 and 1543 cm^{-1}, respectively. The band at 1454 cm^{-1} can be assigned to vibrations of aromatic double bonds. The vibrations of etheric bonds can be seen at 1269 and 1126 cm^{-1}. C–Cl vibration also emerged at 752 cm^{-1}. ^{1}H NMR spectrum of 7**m** identified a peak with an integral of three protons for one CH_3 group as singlet and three protons as singlet for another CH_3 group. Additionally, 14 protons

Table 2 Production of 1-(benzothiazolylamino) methyl-2-naphtols using Ch@GO-DETA.MSA nanocomposite

Entry	Aldehyde	Products	Time (min)	Yield[a] (%)	M.p (°C)	
					Found	Report
1	C_6H_5	**7a**	10	95	202–204	200–202 [56]
2	4-ClC_6H_4	**7b**	10	95	210–212	209–213 [56]
3	4-MeC_6H_4	**7c**	15	92	185–187	182–184 [57]
4	4-FC_6H_4	**7d**	20	92	174–175	174–176 [56]
5	4-$MeOC_6H_4$	**7e**	20	90	174–175	172–174 [56]
6	3-$O_2NC_6H_4$	**7f**	30	96	192–194	190–192 [58]
7	2,4-$Cl_2C_6H_4$	**7g**	25	90	208–209	206–207 [56]
8	3-$MeOC_6H_4$	**7h**	20	91	185–187	184–186 [59]
9	3-BrC_6H_4	**7i**	10	98	202–203	203–205 [60]
10	2-ClC_6H_4	**7j**	15	92	199–200	197–199 [56]
11	2-$NO_2C_6H_4$	**7k**	15	91	217–219	218–220 [56]
12	2,3-$Cl_2C_6H_4$	**7l**	15	91	201–202	200–202 [56]
13	3,4-$(MeO)_2C_6H_4$	**7m**	20	88	176–179	176–178 [56]
14	4-$ClC_6H_4NHCO_2CH_2C_6H_4$	**7n**	30	90	187–189	This work

[a]Isolated yield

were observed for the aromatic region and one proton for the methine group as multiplet in the ^{1}H NMR spectrum. Also, one proton was detected for NH of benzothiazole as singlet and one proton was observed for the 2-naphthol hydroxyl group as a singlet. Also, ^{13}C NMR spectrum determined two methyl carbons, one methine carbon and 22 carbons for aromatic region. Thus, FTIR and NMR spectroscopy verified the structure of **7m**.

Ultimately, the FTIR spectrum of **7n** showed the stretching vibration of NH and OH at 3541 and 3399 cm^{-1}, respectively. Also, the vibration of the amide carbonyl group can be observed at 1690 cm^{-1}, whereas the vibration of aromatic double bonds emerged at 1593 and 1443 cm^{-1}. Further, the bands related to the ether groups can be seen at 1269 and 1177 cm^{-1} and the vibration of the aromatic C–Cl bond was detected at 752 cm^{-1}. Moreover, the ^{1}H NMR spectrum showed two protons for the methylene group as singlet, 18 aromatic protons, and one methine proton as multiplet. Also, two NH protons were identified as singlet and one hydroxyl proton as a singlet. On the other hand, the ^{13}C NMR spectrum reported two aliphatic carbons and 14 aromatic and carbonyl carbons. In addition, elemental analysis confirmed the elemental composition of **7n**. Thus, FTIR and NMR spectroscopy and elemental analysis confirmed the structure of **7n**.

Reaction mechanism

Scheme 7 shows the reaction mechanism. At first, the aldehyde (**5**) was protonated by the acidic (weak) hydrogen of the ammonium group to reach protonated

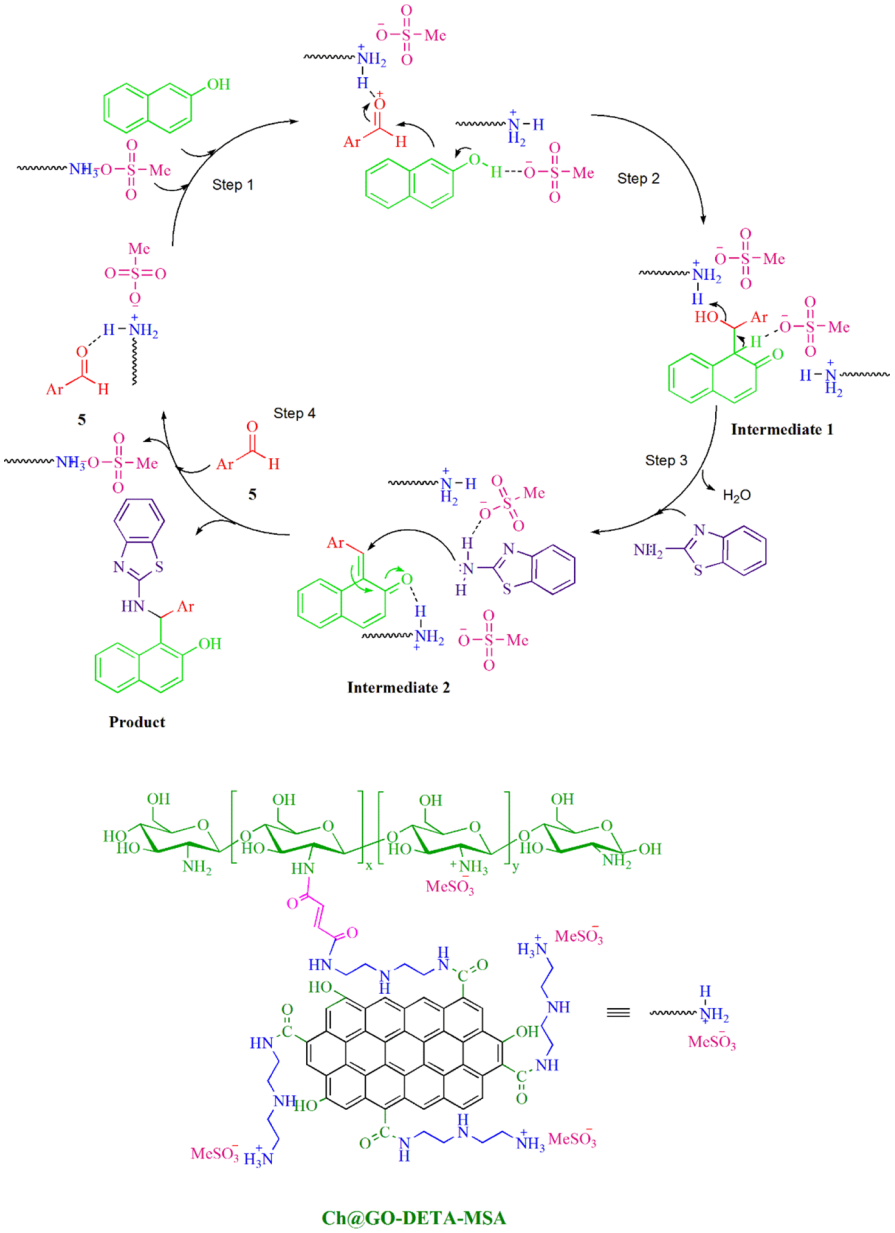

Scheme 7 A plausible mechanism for producing 1-(benzothiazolylamino) methyl-2-naphtols using Ch@GO-DETA.MSA nanocomposite

aldehyde. Then, the anionic part of the nanocomposite (methanesulfonate) contributed to removing the proton of 2-naphthol hydroxide (step 1). In step 2, activated 2-naphthol attacked the activated aldehyde group via a nucleophilic attack to

afford intermediate 1. Furthermore, in step 3 a water molecule was removed and utilized by the acidic and basic sites of the nanocomposite to obtain intermediate 2. Step 4 involved the activation of nitrogen of benzothiazole by methanesulfonate group and its attack on the intermediate 2. Finally, 2-naphthol was protonated by the nanocomposite, which eventually led to the production of 1-(benzothiazole amino) methyl-2-naphthols.

Reusability of nanocomposite

To evaluate and demonstrate the reusability and stability of Ch@GO-DETA.MSA nanocomposite, a one-pot reaction of 2-naphtole, 2-aminobenzothiazole, and 4-chloro benzaldehyde was carried out for five runs under optimized conditions (Fig. 9). The nanocomposite was isolated, washed several times (ethyl acetate), and then dried under vacuum. In agreement with Fig. 9, the yield of the product did not substantially change after five times, suggesting the stability and durability of the nanocomposite.

Superiority over other catalytic systems

The synthesis of 1-((benzo[d]thiazol-2-ylamino) methyl) naphthalen-2-ols was previously reported. Table 3 shows the comparison of the present protocol with those reported in the literature. Based on the data collected, the Ch@GO-DETA.MSA nanocomposite is superior over other catalysts in terms of catalyst load, reaction time, temperature, product yield, environmental compatibility, and workup simplicity.

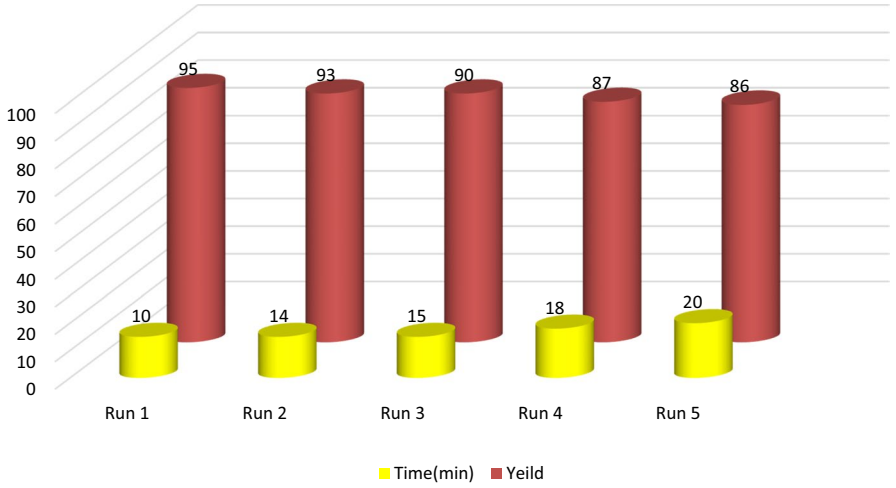

Fig. 9 The results of recyclability and reusability of Ch@GO-DETA.MSA nanocomposite

Table 3 Production of 1-(benzo[d]thiazol-2-ylamino) (phenyl) methyl) naphthalen-2-ol (**7a**) using diverse catalytic systems

Entry	Catalyst	Solvent	Temperature (°C)	Time (Min.)	Yield[a] (%) [Ref.]
1	Fe_3O_4@SiO_2–$ZrCl_2$-MNPs (0.030 g)	Solvent-free	100	15	90 [61]
2	$[(CH_2)_3SO_3HMIM][HSO_4]$ (10 mol%)	Solvent-free	100	5	87 [62]
3	Maltose (20 mol%)	Solvent-free	80	10	89 [63]
4	[H-Suc]HSO_4 (0.030 g)	Solvent-free	80	6	93 [64]
5	Oxalic acid (20 mol%)	Solvent-free	80	10	95 [65]
6	$NaHSO_4.H_2O$ (10 mol%)	Solvent-free	100	10	88 [34]
7	Citric acid (20 mol%)	Solvent-free	80	7	92 [66]
8	IL-SO_3H (3 mol%)	Solvent-free	100	5	91 [60]
9	This catalyst (0.028 g)	Solvent-free	80	10	95 [This work]

The reactions were carried out by the condensation of 2-naphthol, 2-aminobenzothiazole, and benzaldehyde

[a]Isolated yield

Experimental

Chemicals and instruments

The materials were purchased from Merck and Fluka. TLC monitoring was carried out using silica gel SIL G/UV 254 plates. A Thermo Scientific 9200 apparatus was utilized for the measurement of melting points. A Shimadzu model IRPerstige-21 spectrometer was used to record IR spectra. Also, the Shimadzu model: XRD 6000 apparatus was employed to obtain XRD patterns. The particle morphology was examined by the TESCAN electron microscope. Thermal gravimetric analysis (TGA) was carried out at 25 to 600 °C under Ar atmosphere and heating rate of 10 °C min^{-1} using a TA apparatus (model Q 600). Elemental analysis was performed by a CHN-O-Rapid Heraeus elemental analyzer. Additionally, a Bruker Avance 500 spectrometer was utilized to record NMR spectra, while an Agilent Technologies 5975C spectrometer was applied to obtain mass spectra using an MSD detector run at ionization potential of 20 to 70 eV.

Synthesis of modified graphene oxide, chitosan-g-maleic anhydride, and methane sulfonic acid (Ch@GO-DETA.MSA) nanocomposite

Production of diethylenetriamine-functionalized GO (GO@DETA)

GO was produced according to the modified Hammer's method (Scheme 1) [38]. Diethylenetriamine was also functionalized with graphene oxide according to our previous work (Scheme 1) [36]. Typically, graphene oxide (1.5 g) in dimethylformamide (30 mL) was sonicated in a 50-ml flask for 1 h at 30 °C using an ultrasonic bath. Subsequently, diethylenetriamine (1 ml), triethylamine (1 mL), and

dicyclohexyl carbodiimide (DCC, 1 g) were charged and spun at 25 °C for 48 h. Finally, distilled water (2 mL) and DMSO (20 mL) were charged and hot-filtered. In the end, they were washed with hot alcohol and dried at room temperature to obtain GO@DETA.

Synthesis of chitosan grafted maleic anhydride (Ch@MA)

A mixture of chitosan (1 g), N-methylpyrrolidine (NMP, 30 mL), and maleic anhydride (0.1 g) was heated at 90 °C for 20 h under N_2. After cooling, the resulting solid powder was filtered and purified by washing with ethanol and dried under vacuum to afford chitosan-g-maleic anhydride (Scheme 2).

Preparation of modified graphene oxide and chitosan-g-maleic anhydride (Ch@GO-DETA) nanocomposite

NMP (20 mL) was added to Ch@MA (1 g), and dispersion was sonicated for 60 min at 60 °C using an ultrasonic bath. Similarly, the dispersion of GO@DETA (0.4 g) in NMP (20 mL) was prepared and sonicated for 1 h at 50 °C. Then, the GO@DETA colloidal solution was added to the chitosan solution. Moreover, after stirring combined solution for 10 min at room temperature, EDC (0.3 g) was charged and the reaction continued for 24 h at 130 °C. Finally, deionized water (30 mL) and alcohol (20 mL) were charged, centrifuged, and rinsed by alcohol and deionized water, followed by drying to afford Ch@GO-DETA nanocomposite (Scheme 2).

Synthesis of modified graphene oxide, chitosan-g-maleic anhydride, and methane sulfonic acid (Ch@GO-DETA.MSA) nanocomposite

To CH@GO-DETA (1 g), dry chloroform (15 mL) was charged and sonicated for 30 min. After adding methane sulfonic acid (0.5 mL), the stirring was maintained for 5 h. Ultimately, the matrix was centrifuged, rinsed with chloroform (2 × 15 mL), and dried at room temperature to afford Ch@GO-DETA.MSA nanocomposite (Scheme 3).

Synthesis of 4-[4-(4-chlorophenyl)-3-aza-2-oxo-propyloxy] benzaldehyde (3)

To N-(4-chloroaniline)-2-chloroacetamide (**1** [55], 1 mmol, 0.247 g) in acetonitrile (25 mL) were added 4-hydroxy benzaldehyde (**2**, 1 mmol, 0.122 g) and potassium carbonate (1 mmol, 0.14 g) (Scheme 4). The mixture was refluxed for 48 h under N_2. The progress was monitored using thin-layer chromatography (TLC). Deionized water (60 mL) was added, and after filtration, the resulting crude was recrystallized in alcohol to afford **3** in 92% yield. m.p. 120–121°C, FTIR (KBr) υ: 3541, 3398, 1689, 1593, 1534, 1442, 1330, 1269, 1238, 1176, 817, 752 cm^{-1}. ^1H NMR (500 MHz, DMSO-d_6) δ 4.87 (s, 2H, CH_2), 7.19 (d, $J = 8.1$ Hz, 2H), 7.39 (d, $J = 8.2$ Hz, 2H), 7.68 (d, $J = 8.1$ Hz, 2H), 7.90 (d, $J = 8.2$ Hz, 2H), 9.74 (s, 1H, NH), 9.88 (s, 1H, COH); ^{13}C NMR (125 MHz, DMSO-d_6) δ 66.5, 113.8, 114.6, 120.7,

126.7, 128.1, 128.6, 129.5, 131.2, 131.2, 136.8, 162.1, 165.5, 189.7, 190.7; MS (EI): m/z 290 $(M+1)^+$.

General procedure for the preparation of 1-(benzothiazolylamino) methyl-2-naphtols

For optimization, 4-chlorobenzaldehyde (1.0 mmol, 0.15 g), 2-aminobenzothiazole (1.0 mmol, 0.15 g), and 2-naphtol (1.0 mmol, 0.14 g) were charged to Ch@GO-DETA.MSA (0.028 g) (Scheme 5). The process was carried out under various conditions, and the influence of four variables including time, reaction temperature, catalyst load, and solvent (or solvent-free condition) was investigated. Ultimately, the optimum conditions were defined as the reaction temperature of 80 °C, catalyst load of 0.028 g, solvent-free medium, and reaction time of 10 min (Table 1).

The process was detected using TLC (n-hexane/ethyl acetate) (4:1). The precipitate was dispersed in alcohol, the nanocomposite was collected, and the precipitates were rinsed with ethyl acetate several times followed by drying under vacuum.

Selected spectral data of products

1-(Benzo[d]thiazol-2-ylamino) (4-chlorophenyl) methyl) naphthalen-2-ol (7e)

^{1}H NMR (DMSO-d_6) δ 7.02–7.81 (m, 15H, ArH, and 1H, methine), 8.87 (s, 1H, NH), 10.23 (s, 1H, OH); ^{13}C NMR (125 MHz, DMSO-d_6) δ 53.3, 118.8, 119.0, 121.5, 121.7, 123.1, 124.2, 124.3, 126.0, 127.0, 128.5, 128.6, 129.2, 130.4, 131.3, 131.4, 132.6, 142.2, 152.5, 153.8, 158.2, 163.1, 166.8.

1-((Benzo[d]thiazol-2-ylamino) (2,3-dichlorophenyl) methyl) naphthalen-2-ol (7l)

^{1}H NMR (500 MHz, DMSO-d_6) δ 7.04–8.07 (m, 14H, 13H, Ar, 1H, methine CH), 8.97 (s, 1H, NH), 9.99 (s, 1H, OH).

1-(Benzo[d]thiazol-2-ylamino) (3,4-dimethoxyphenyl) methyl) naphthalen-2-ol (7m)

IR (KBr, cm^{-1}): 3368, 2932, 1771, 1543, 1454, 1331, 1269, 1126, 822, 752; ^{1}H NMR (500 MHz, DMSO-d_6) δ 3.61 (s, 3H, CH_3), 3.67 (s, 3H, CH_3), 6.76–7.96 (m, 15H, 14H, Ar, and s, 1H, methine), 8.82 (s, 1H), 10.16 (s, 1H); ^{13}C NMR (125 MHz, DMSO-d_6) δ 53.7, 53.8, 56.1, 111.2, 111.3, 112.2, 118.6, 119.1, 119.3, 121.4, 121.5, 123.0, 124.4, 126.0, 126.7, 129.1, 130.0, 131.2, 132.8, 135.2, 148.1, 149.1, 152.7, 153.7, 166.8.

2-(4-((Benzo[d]thiazol-2-ylamino) (2-hydroxynaphthalen-1-yl) methyl) phenoxy)-N-(4-chlorophenyl) acetamide (7n)

IR (KBr, cm^{-1}): 3541, 3399, 3063, 2924, 1690, 1593, 1443, 1331, 1269, 1177, 818, 752; ^{1}H NMR (500 MHz, DMSO-d_6) δ 4.15 (s, 2H, CH_2), 6.43–7.38 (m, 19H, 18H

Ar, and 1H methine), 8.30 (s, 2H, 2NH), 9.69 (s, 1H, OH); ^{13}C NMR (125 MHz, DMSO-d_6) δ 53.0, 67.3, 114.5, 118.2, 118.6, 118.8, 121.0, 121.1, 121.5, 123.1, 124.0, 125.5, 126.3, 127.4, 128.7, 129.6, 130.8, 132.2, 133.4, 135.2, 137.4, 137.9, 152.3, 153.3, 156.4, 166.4, 166.9; Anal. Calcd for $C_{32}H_{24}ClN_3O_3S$: C, 67.90; H, 4.27; N, 7.42%. Found: C, 67.81; H, 4.36; N, 7.53%.

Conclusion

An efficient procedure is introduced for the production of 1-(benzothiazolylamino) methyl-2-naphthols (potentially interesting and biologically active heterocycles) using a novel green nanocomposite bearing chitosan and graphene oxide. The encouraging benefits of this protocol include moderate condition, fast reaction rates, generality, convenient purification stage, inexpensive promoter, nontoxicity, and easy handling of catalyst and efficiency. The developed protocol follows the green chemistry principles and can be used for designing novel chitosan–graphene nanocomposites for organic synthesis procedures and materials science.

Supplementary Information The online version contains supplementary material available at https://doi.org/10.1007/s11164-021-04538-z.

Acknowledgements The authors would like to appreciate the Payame Noor University (PNU) Research Council for supporting this research study.

Declarations

Conflict of interest There are no conflicts of interest to declare.

References

1. A. Dhakar, R. Goyal, A. Rajput, M. Singh Kaurav, V.S. Tomar, D. Agarwal, Curr. Chem. Lett. **8**, 125 (2019)
2. P.-L. Wang, S.-Y. Ding, Z.-C. Zhang, Z.-P. Wang, W. Wang, J. Am. Chem. Soc. **141**, 45 (2019)
3. A. de Fátima, S. Barreto, C.K.Z. Andrade, Beilstein J. Org. Chem. **15**, 906 (2019)
4. Q. Xiong, S. Dong, Y. Chen, X. Liu, X. Feng, Nat. Commun. **10**, 1 (2019)
5. S. Yu, R. Hua, X. Fu, G. Liu, D. Zhang, Sh. Jia, H. Qiu, W. Hu, Org. Lett. **21**, 5737 (2019)
6. M. Ahmadi, L. Moradi, M. Sadeghzadeh, Monatsh Chem. **150**, 1111 (2019)
7. S. Naeim-Fallahiyeh, E. Rostami, H. Golchaman, S. Kaman-Torki, Res. Chem. Intermed. **46**, 4141 (2020)
8. N.G. Khaligh, T. Mihankhah, M.R. Johan, Synth. Commun. **49**, 1334 (2019)
9. Y. Guo, X. Sun, Y. Liu, W. Wang, H. Qiu, J. Gao, Carbon **50**, 2513 (2012)
10. U. Siripatrawan, P. Kaewklin, Int. J. Biol. Macromol. **112**, 523 (2018)
11. M. Motiei, S. Kashanian, L.A. Lucia, M. Khazaei, J. Control. Release **260**, 213 (2017)
12. L. Shahriary, A. Athawale, Int. J. Renew. Energy Environ. Eng. **2**, 58 (2014)
13. N. Zhang, H. Qiu, Y. Liu, W. Wang, Y. Li, X. Wang, J. Gao, J. Mater. Chem. **21**, 11080 (2011)
14. P. Choudhury, P. Ghosh, B. Basu, Mol. Divers. **24**, 283 (2020)
15. A. Singh, G. Sinsinbar, M. Choudhary, V. Kumar, R. Pasricha, H.N. Verma, S.P. Singh, K. Arora, Sens. Actuators B Chem. **185**, 675 (2013)
16. N. Baig, D.S. Chauhan, T.A. Saleh, M.A. Quraishi, New J. Chem. **43**, 2328 (2019)
17. J.N. Jebaranjitham, C. Mageshwari, R. Saravanan, N. Mu, Compos. Part B Eng. **171**, 302 (2019)

18. M. Khandelwal, S.H. Hur, J.S. Chung, Chem. Eng. J. **363**, 120 (2019)
19. H. Al Muhaimeed, J. Int. Med. Res. **25**, 175 (1997)
20. A. Carpio, J. Neurol. Neurosurg. Psychiatry **66**, 411 (1999)
21. J.E. Richter, Am. J. Gastroenterol. **92**, S30 (1997)
22. P. Winstanley, Lancet **352**, 1080 (1998)
23. E.R. Atkinson, F.E. Granchelli, J. Pharm. Sci. **65**, 618 (1976)
24. A. Catalano, A. Carocci, I. Defrenza, M. Muraglia, A. Carrieri, F.V. Bambeke, A. Rosato, F. Corbo, C. Franchini, Eur. J. Med. Chem. **64**, 357 (2013)
25. V.N. Telveka, V.K. Bairwa, K. Satardekar, A. Bellubi, Bioorg. Med. Chem. Lett. **22**, 649 (2012)
26. D. Fajkusova, M. Pesko, S. Keltosova, J. Guo, Z. Oktabec, M. Vejsova, P. Kollar, A. Coffey, J. Csollei, K. Kralova, J. Jampilek, Bioorg. Med. Chem. **20**, 7059 (2012)
27. S.N. Manjula, N.M. Noolvi, K.V. Parihar, S.A.M. Reddy, V. Ramani, A.K. Gadad, G. Singh, N.G. Kutty, C.M. Rao, Eur. J. Med. Chem. **44**, 2923 (2009)
28. S.U. Mestry, D.M. Patil, S.T. Mhaske, Polym. Bull. **76**, 1899 (2019)
29. M.-A. Zolfigol, M. Navazeni, M. Yarie, R. Ayazi-Nasrabadi, Res. Chem. Intermed. **44**, 191 (2017)
30. M. Seddighi, F. Shirini, M. Mamaghani, C. R. Chim. **18**, 573 (2015)
31. A. Moradi, R. Heydari, M.-T. Maghsoodlou, Res. Chem. Intermed. **41**, 7377 (2015)
32. S. Javanshir, A. Ohanian, M.-M. Heravi, M.R. Naimi-Jamal, F. Bamoharram, J. Saudi. Chem. Soc. **18**, 502 (2011)
33. O. Goli-Jolodar, F. Shirini, M. Seddigh, RSC Adv. **6**, 43844 (2016)
34. A. Hosseinian, H.-R. Shaterian, Phosphorus Sulfur Silicon Relat. Elem. **187**, 1056 (2012)
35. P. Ajitha, K. Vijayalakshmi, M. Saranya, T. Gomathi, K. Rani, P.N. Sudha, A. Sukumaran, Int. J. Boil. Macromol. **104**, 1469 (2017)
36. E. Rostami, S.M. Haghayeghi, Iran. J. Catal. **11**, 37 (2021)
37. W.S. Hummers, R.E. Offeman, J. Am. Chem. Soc. **80**, 1339 (1958)
38. J. Chen, B. Yao, C. Li, G. Shi, Carbon **64**, 225 (2013)
39. M. Namvari, H. Namazi, Int. J. Environ. Sci. Technol. **11**, 1527 (2014)
40. Y.H. Khan, A. Islam, A. Sarwar, N. Gull, S.M. Khan, M.A. Munawar, S. Zia, A. Sabir, M. Shafiq, T. Jamil, Carbohydr. Polym. **146**, 131 (2016)
41. N. Shang, C. Feng, H. Zhang, S. Gao, R. Tang, C. Wang, Z. Wang, Catal. Commun. **40**, 111 (2013)
42. I. Abdurrahim, Heliyon **5**, e02342 (2019)
43. M.F. Queiroz, K.R.T. Melo, D.A. Sabry, G.L. Sassaki, H.A.O. Rocha, Mar. Drugs **13**, 141 (2015)
44. M. Hosseini, M. Montazer, R. Damerchely, J. Eng. Fibers Fabr. **8**, 25 (2013)
45. M. Antunes, M.T. Donato, V. Paz, F. Caetano, L. Santos, R. Colaço, L.C. Branco, B. Saramago, Tribol. Lett. **68**, 1 (2020)
46. M. Gierszewska-Drużyńska, J. Ostrowska-Czubenko, Prog. Chem. Appl. Chitin. Deriv. **20**, 43 (2015)
47. M. Pieróg, J. Ostrowska-Czubenko, M. Gierszewska-Drużyńska, Prog. Chem. Appl. Chitin. Deriv. **17**, 71 (2012)
48. Z.R. Dizavandi, A. Aliakbar, M. Sheykhan, Electrochim. Acta **227**, 345 (2017)
49. W. Monnens, C. Deferm, K. Binnemans, J. Fransaer, Phys. Chem. Chem. Phys. **22**, 24526 (2020)
50. S. Ganesan, G.P. Halliah, Orient. J. Chem. **35**, 1789 (2019)
51. S. Sayyar, E. Murray, B.C. Thompson, J. Chung, D.L. Officer, S. Gambhir, G.M. Spinks, G.G. Wallace, J. Mater. Chem. B **3**, 481 (2015)
52. D. Han, L. Yan, W. Chen, W. Li, Carbohydr. Polym. **83**, 653 (2011)
53. H. Hu, X. Wang, J. Wang, F. Liu, M. Zhang, C. Xu, Appl. Surf. Sci. **257**, 2637 (2011)
54. Z. Jafari, A.S. Rad, R. Baharfar, S. Asghari, M.R. Esfahani, J. Mol. Liq. **315**, 113835 (2020)
55. M. Saeedi, F. Goli, M. Mahdavi, G. Dehghan, M.A. Faramarzi, A. Foroumadi, A. Shafiee, Iran J. Pharm. Res. **13**, 881 (2014)
56. P.K. Kalavagunta, P.K. Bagul, A. Jallapally, S. Kantevari, S.K. Banerjee, N. Ravirala, Eur. J. Med. Chem. **83**, 344 (2014)
57. A. Shaabani, A. Rahmati, E. Farhangi, Tetrahedron Lett. **48**, 7291 (2007)
58. L. Yang, E. J. Chem. **9**, 2424 (2012)
59. A. Kumar, M.-S. Rao, V.-K. Rao, Aust. J. Chem. **63**, 1538 (2010)
60. H.R. Shaterian, A. Hosseinian, Sci. Iran. **21**, 727 (2014)
61. F. Kamali, F. Shirini, Appl. Organomet. Chem. **32**, e3972 (2018)
62. H.R. Shaterian, A. Hosseinian, Res. Chem. Intermed. **41**, 793 (2015)
63. B. Adrom, M.T. Maghsoodlou, N. Hazeri, M. Lashkari, Res. Chem. Intermed. **41**, 7553 (2015)

64. O. Goli-Jolodar, F. Shirini, J. Iran. Chem. Soc. **13**, 1077 (2016)
65. M.T. Maghsoodlou, M. Karima, M. Lashkari, B. Adrom, J. Aboonajmi, J. Iran. Chem. Soc. **14**, 329 (2017)
66. M. Lashkari, M.T. Maghsoodlou, M. Karima, B. Adrom, M. Fatahpour, Acta Chemica Iasi **24**, 112 (2016)